Ocean Engineering 291 (2024) 116447

Contents lists available at ScienceDirect

Ocean Engineering

journal homepage: www.elsevier.com/locate/oceaneng

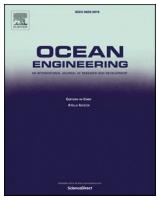

Research paper

Hydrodynamics of a Remora-inspired autonomous underwater vehicle approaching and docking to a benchmark submarine

Yunxin Xu [a], Weichao Shi [b,*], Yang Song [a], Hongbo Hou [a]

[a] Department of Naval Architecture, Ocean & Marine Engineering, University of Strathclyde, UK
[b] School of Engineering, Newcastle University, UK

ARTICLE INFO

Handling Editor: Prof. A.I. Incecik

Keywords:
Computational fluid dynamics
Autonomous underwater vehicle
Dynamic dockng
Drag reduction
Biomimetics

ABSTRACT

Autonomous underwater vehicles (AUVs) are applied in a variety of industries to increase the efficiency and safety of maritime operations. Traditional docking and recovery techniques for AUVs, however, can be inefficient. Therefore, the development of a dynamic underwater recovery mechanism for AUVs is now needed.

Recent research has investigated the symbiotic relationship between the remora fish and the shark from a hydrodynamic perspective. Numerical simulations have demonstrated that by exploiting the boundary layer and adverse pressure gradient regions around the shark, the resistance experienced by remora fish can be significantly reduced. Inspired by this, an AUV was designed, and numerical simulations were conducted to investigate the impact of various attachment locations. Moreover, simulations were performed to investigate the hydrodynamic characteristics of the AUV during the docking process, specifically when it enters the boundary layer of the submarine and approaches it. The boundary layer flow, which influences the AUV's resistance, can also provide a force that attract the AUV towards the submarine.

This research identifies an optimal attachment location and investigates the effects on the AUV when two underwater vehicles of significantly different sizes are in close proximity. It supports further study to develop a dynamic underwater docking operation.

1. Introduction

Autonomous underwater vehicles (AUVs) are now widely used across a range of industries, including ocean surveying, surveillance, pipeline inspection, treasure hunting, and search and rescue missions (Schofield et al., 2007; Kemna et al., 2011; Forrest et al., 2008; Fernandes et al., 2015; Zhang et al., 2013; Venkatesan, 2016). Despite their many benefits, recovering AUVs remains one of the riskiest stages of a mission and the development of reliable recovery technology still faces several obstacles (Nicholson and Healey, 2008; Hardy and Barlow, 2008; Hayashi et al., 2013; Heo et al., 2017). The traditional method for recovering AUVs involves a surface mothership travelling to the location where the AUV sends a GPS signal, and then using an 'A'-frame or onboard crane to retrieve the AUV. However, this method presents several challenges, such as the need for precise location information and the difficulty of recovering AUVs in adverse weather conditions without causing damage (Hardy and Barlow, 2008).

On the other hand, researchers and engineers are trying to avoid frequent retrieval for charging and communication. Therefore there is a growing trend for the development of underwater docking stations to support data transfer and charging. For example, a solution developed by Singh et al. (2001) using acoustic ultrashort baseline technology can guide and allow AUV docking from any underwater direction. However, this kind of docking station is generally stationary and it can only be used in known areas. Recently, Sarda and Dhanak presented a concept of an unmanned surface vehicle to automatically launch and recover the Remus 100 (Sarda and Dhanak, 2016), and this technique used unmanned aerial vehicles (UAVs) to operate and guide the recovery. But these solutions are all performed stationarily. At the moment, there is no efficient method for performing dynamic recovery for AUVs.

To tackle this challenging problem of dynamic AUV recovery, a natural cooperative relationship observed between remora fish and sharks is inspiring. Remora fish, also referred to as "suckerfish," exhibit a unique attachment behaviour and are often found attached to a host rather than swimming independently. The fish attach to their hosts in order to travel and forage, due to their limited swimming abilities. The attachment position of remora fishes on the body of sharks is not randomly selected (Brunnschweiler, 2006; Beckert et al., 2016; Silva-

* Corresponding author. School of Engineering, Newcastle University, Armstrong Building, Newcastle upon Tyne, NE1 7RU, UK.
E-mail address: weichao.shi@newcastle.ac.uk (W. Shi).

https://doi.org/10.1016/j.oceaneng.2023.116447
Received 7 May 2023; Received in revised form 9 June 2023; Accepted 25 November 2023
Available online 7 December 2023

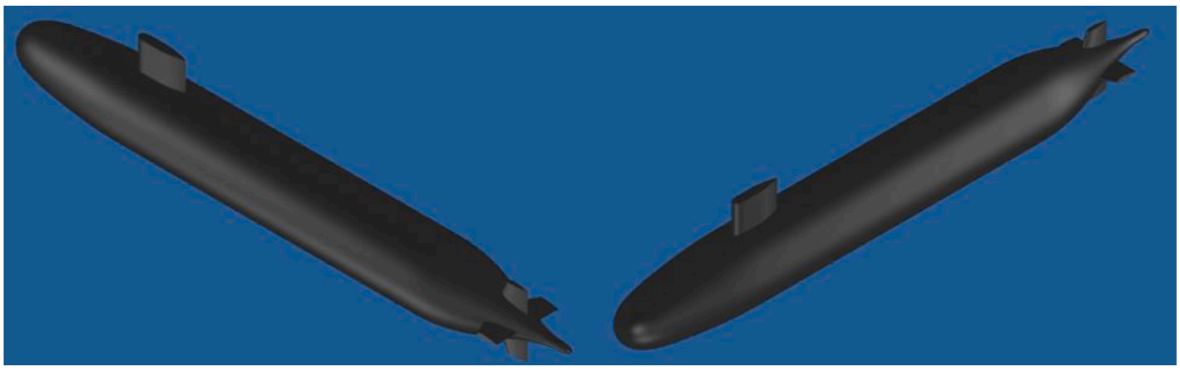

Fig. 1. The 3D geometry of the DARPA Suboff AFF-8 submarine model.

Table 1
The basic parameters of the DARPA Suboff AFF-8 submarine models.

Main Particular	Model Scale	Full Scale
Scale	24	1
Length (m)	4.356	104.544
Maximum Diameter (m)	0.508	12.192

Table 2
The basic parameters of the INSEAN E1619 propeller models.

Main Particular	Model Scale	Full Scale
Scale	13	1
Diameter (m)	0.485	6.288
Number of Blades	7	

and Sazima, 2006). From a hydrodynamic perspective, when remora fish attaches to a shark, the boundary layer and adverse pressure gradient regions around the shark can significantly reduce resistance for remora fishes in specific attachment locations. Specifically, at the back and belly attachment locations of the shark, the resistance reduction rate increased with the increasing forward speed of the host. Additionally, it should be noted that due to the incoming flow being blocked by the dorsal fin and shark body and adverse pressure gradients generated behind them, a forward thrust was provided for the remora fish(Xu et al., 2021).

Therefore, the distinctive behaviours of remora fish were utilized as inspiration for this study of an underwater AUV dynamic recovery system, where another large underwater vehicle acts as a mother ship for the recovery system. Leong et al. (Leong et al., 2015) presented a study on the hydrodynamic interaction effects between an AUV and a submarine operating in close proximity. The findings revealed that the AUV was attracted towards the submarine around the stern of the submarine and pushed away near the bow. In the midship region of the submarine, the interaction effect was found to be minimal. However, there has been relatively little attention given to the interaction between two underwater vehicles of significantly different sizes, particularly when the two vehicles are in close proximity to each other.

Under this research framework, this study employed the Computational Fluid Dynamics (CFD) method to investigate the hydrodynamic possibility of a remora-inspired AUV dynamically docking onto a benchmark submarine. First, a remora-inspired AUV hull has been designed for the first time. Then a systematic study has been conducted to investigate different docking positions. Then, a fully coupled analysis has been conducted to investigate the hydrodynamics with the developed AUV approaching and docking to the submarine.

2. Model information and geometry preparation

This section provides a detailed description of the simulated models used in the study. The benchmark submarine model is the open-source DARPA Suboff AFF-8 submarine model with the INSEAN E1619 propeller model. The remora-inspired AUV model is in-house developed inspired by the remora.

2.1. The DARPA suboff AFF-8 submarine

DAPRA Suboff submarine model is a widely recognized benchmark model with the available research on its performances in both model and full scale conditions (Liu and Huang, 1998; Roddy, 1990; Sezen et al.,

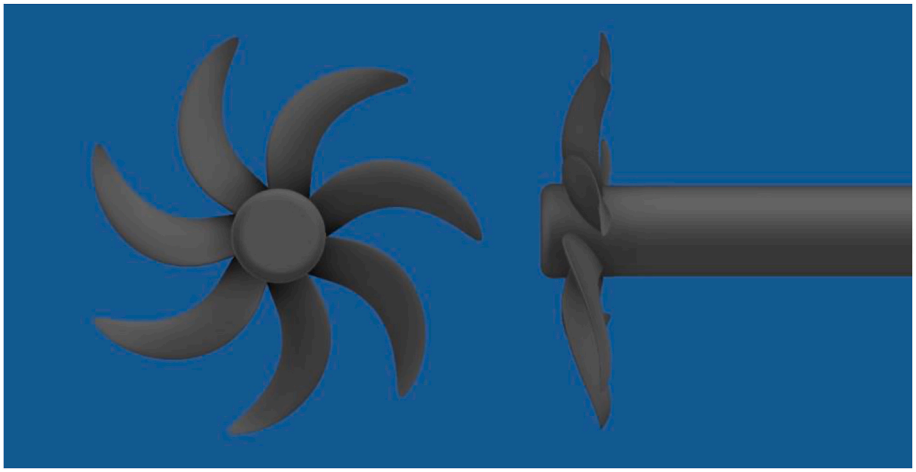

Fig. 2. The 3D geometry of the INSEAN E1619 propeller model.

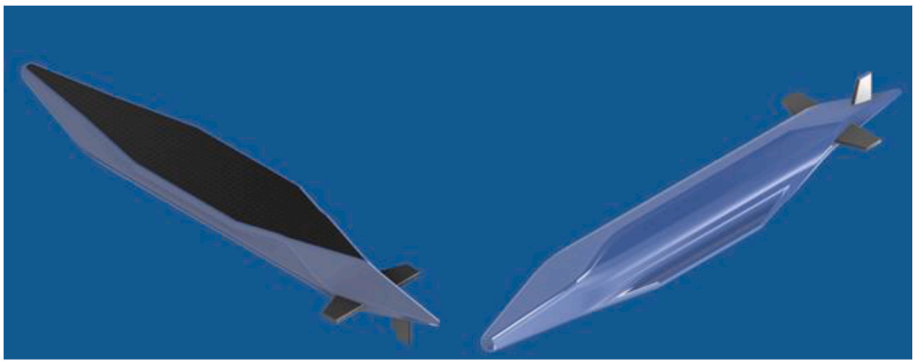

Fig. 3. The 3D geometry of the remora-inspired AUV models.

Table 3
The basic parameters of the remora-inspired AUV models.

Main Particular	
Hull Length (m)	2.000
Hull Width (m)	0.320
Hull Height (m)	0.210

2018; Chase and Carrica, 2013). It is used as the mother vehicle for this investigation. In this study, considering that the presence of appendages such as the sail and rudders can significantly affect the flow around the submarine, the fully appended model, called AFF-8, was utilized. Fig. 1 illustrates the 3D geometry of the DARPA Suboff AFF-8 submarine model, while the key parameters are provided in Table 1.

2.2. The INSEAN E1619 propeller

Chase and Carrica (2013) and Sezen et al. (Sezen et al., 2018) have previously conducted studies using the INSEAN E1619 propeller with the DARPA Suboff AFF-8 submarine model at full-scale and model-scale conditions. This study continued to use the same propeller for the self-propulsion simulations. The propeller was mounted at the stern of the submarine. Fig. 2 shows the 3D geometry of the INSEAN E1619 propeller model, while Table 2 lists its fundamental parameters.

2.3. The Remora-inspired AUV

Inspired by the remora fish, the AUV used in this study feature a suction disk on one side of its hull to perform the docking operations. The remora-inspired AUV model is presented in Fig. 3, and the basic parameters are shown in Table 3.

3. CFD simulation methodology and validation study

Prior to the research of the remora inspired AUV, the CFD simulation methodology was established and several validation studies using the benchmark submarine model were conducted to gain confidence for the used numerical methodology. Numerical simulations were conducted using the CFD software STAR-CCM + to investigate the hydrodynamic characteristics. A Reynolds-Averaged Navier–Stokes (RANS) model along with a K-ω Shear Stress Transport (K-ω SST) turbulence model which has been extensively utilized in industrial applications (Singh et al., 2011; STAR-CCM + guidelines) is employed in this study. The K-ω

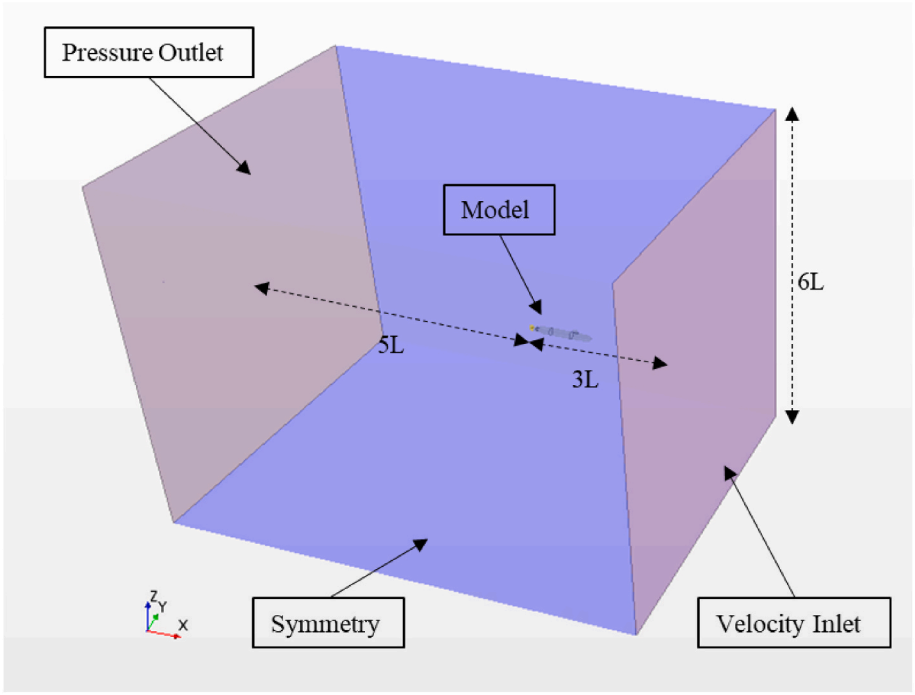

Fig. 4. Domain and boundary conditions of the submarine resistance analysis.

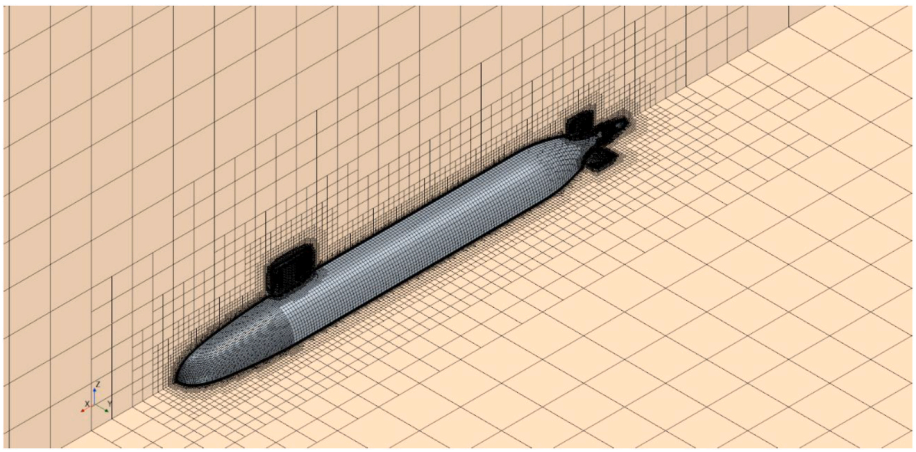

Fig. 5. Mesh view of the model-scale DARPA Suboff AFF-8 submarine model.

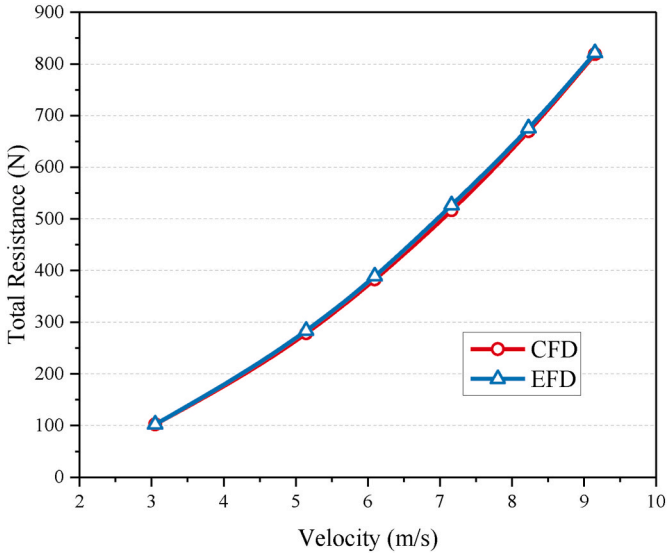

Fig. 6. The comparison of the model-scale DARPA Suboff AFF-8 submarine resistances between the numerical and experimental results.

SST turbulence model offers the benefits of both the standard K-ω turbulence model and K-ε turbulence model. It utilizes the K-ω formulation in the inner parts of the boundary layer to capture complex flow phenomena. Conversely, the K-ε formulation can be applied in regions away from the wall, where the turbulence properties have lower sensitivity (Menter, 1994). In all simulations, the reference altitude was set at the centre of domain, and the density of water was 997.561 kg/m3 with the dynamic viscosity of 8.8871E-4 Pa-s.

3.1. Methodology & validation study I: resistance analysis

First, a resistance analysis for the benchmark submarine was conducted to validate the used CFD simulation methodology. The experimental data of the model-scale DARPA Suboff AFF-8 submarine resistance was provided by Liu and Huang (1998). To perform this analysis, a cuboid computational domain was created as shown in Fig. 4. The recommended dimensions for the computational domain were used (ITTC, 2011). The no-slip wall was used on the full surface, located 3 L (length of the model) from the inlet and the sides, which were defined as the velocity inlet and the symmetry respectively. The outlet was defined as a pressure outlet and located 5 L away from the model.

A volumetric control automatic meshing tool was utilized to generate the mesh for the simulations. The mesh was refined near the models, particularly in the areas of the sail, rudders, stern, and propeller. The detailed mesh scenes can be viewed in Fig. 5, and the cell count was 1.8 million. The wall treatment used in all simulations was the all y + treatment setting in STAR-CCM+. The approach is a hybrid one that employs a high-y + treatment (y+ > 30) for coarse meshes and a low-y + treatment (y+ < 1) for fine meshes (STAR-CCM + guidelines). For the submarine simulations, the average y+ was kept below 1. The fine prism layer mesh, which was 0.2 m thick with 14 layers on the submarine surface was used to resolve the boundary layer.

Table 4
The difference between the numerical and experimental results for the model-scale DARPA Suboff AFF-8 submarine resistance analysis.

Velocity (m/s)	Resistance – CFD (N)	Resistance – EFD (N)	Difference
3.051	102.5	102.3	0.20%
5.144	278.5	283.8	1.87%
6.096	383.0	389.2	1.59%
7.161	516.6	526.6	1.90%
8.231	669.9	675.6	0.84%
9.152	819.1	821.1	0.24%

The inflow velocities used in numerical simulations ranged from 3.051 m/s to 9.152 m/s, which were the same as those used in experimental data. Fig. 6 shows good agreement between the numerical and experimental results, with differences ranging from 0.20% to 1.90% as summarized in Table 4.

3.2. Methodology & validation study II: openwater propeller analysis

With the confidence obtained from the resistance simulation, to validate the propeller simulation, the analysis of the openwater propeller is conducted and compared against the experimental data (Sezen et al., 2018; Di Felice et al., 2009). A cylindrical computational domain with stationery and rotatory regions was created, as shown in Fig. 7. The no-slip wall condition was applied to the propeller model, while the diameter of the domain was set to 10 times the diameter of the propeller (10D). The inlet was defined as a velocity inlet, positioned 4D upstream from the model. A pressure outlet was applied to the outlet, which was 11D downstream from the propeller model. The circumferential face was defined as a symmetry plane. To properly capture the rotation of the propeller, 200 time-steps per revolution were used, as recommended by the ITTC Practical Guidelines for Ship CFD Applications guidelines (ITTC, 2011).

The volumetric control automatic meshing tool and all y + treatment setting also used for these simulations. The mesh scene is proved in

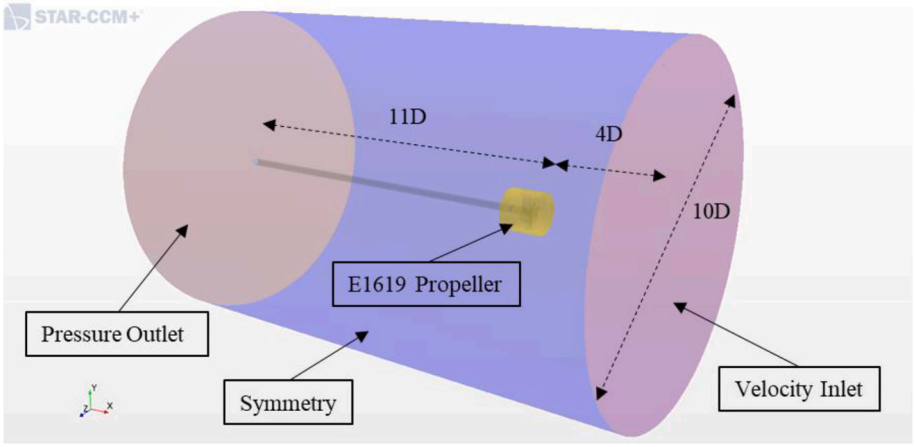

Fig. 7. Domain and boundary conditions of the model-scale and full-scale open water propeller analyses.

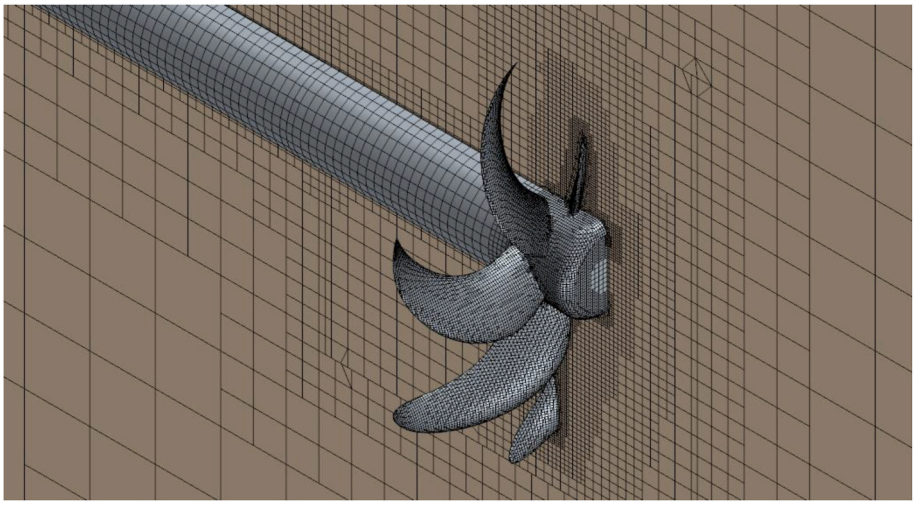

Fig. 8. Mesh view of the INSEAN E1619 propeller model analyses.

Fig. 8. The cell count was 0.59 million and the average y+ was kept above 30.

The numerical results of the open-water analyses for model-scale INSEAN E1619 propellers, which were compared with experimental data provided by INSEAN (Sezen et al., 2018; Di Felice et al., 2009). Nondimensional numbers were utilized to assess the accuracy of the numerical simulation. The advance ratio, J, was calculated with the following Equation (1) (ITTC, 2008):

$$J = \frac{V_a}{n * D}, \qquad \text{Equation 1}$$

where, V_a is the velocity of the inflow, m/s; n is the rotational speed of the propeller in revolutions per second; D is the propeller diameter, m.

The non-dimensional torque coefficients, K_Q, was calculated with the following Equation (2) (ITTC, 2008):

$$K_Q = \frac{Q}{\rho * n^2 * D^5}, \qquad \text{Equation 2}$$

where, Q is the torque, N*m; ρ is the density of the inflow, kg/mˆ3;

And the non-dimensional thrust coefficients, K_T, was calculated with the following Equation (3) (ITTC, 2008):

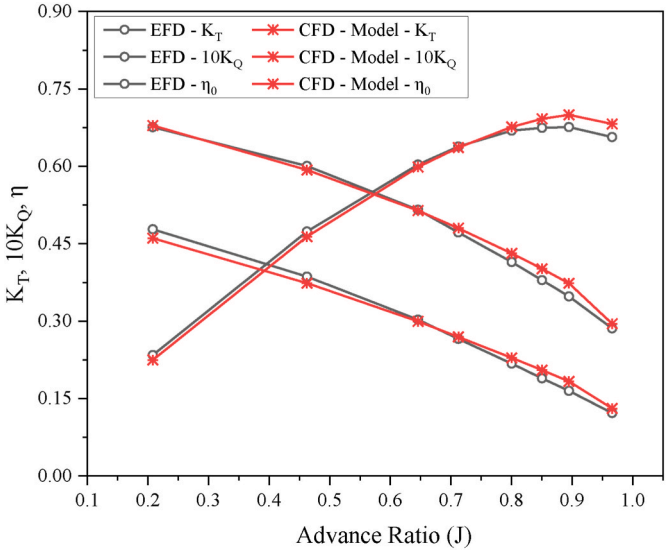

Fig. 9. The Open water performance comparison of the INSEAN E1619 propeller between the numerical and experimental results.

$$K_T = \frac{T}{\rho * n^2 * D^4}, \quad \text{Equation 3}$$

where, T is the thrust, N*m;

The performance curves of the INSEAN E1619 propeller obtained from the numerical and experimental data are compared in Fig. 9. The results indicate a good agreement for model-scale propeller open-water analysis.

3.3. Methodology & validation study III: self-propulsion analysis

With both hull resistance simulation and propeller simulation, to understand the fully developed flow around the submarine hull with propeller action, a full-scale self-propulsion simulation was conducted. Due to the lack of full-scale measurement data, the simulation results were compared with another numerical simulation results by Sezen et al. (Sezen et al., 2021). The same settings like the previous simulations, regarding the computational domain, the boundary conditions and the mesh generation, have been adopted. The detailed mesh scenes can be viewed in Fig. 10 and the cell count was 6.30 million.

The Dynamic Fluid Body Interaction (DFBI) module of CFD software STAR-CCM+ was employed to perform this self-propulsion simulation. In the DFBI model, a propeller speed was predetermined, and the propeller generates the thrust to propel the submarine. The computational domain moves together with the submarine model referring to the submarine local coordinate system. As the submarine moved, the resistance increased with the increased velocity of the submarine until the net horizontal force of thrust and resistance became zero, at which the self-propulsion point could be found.

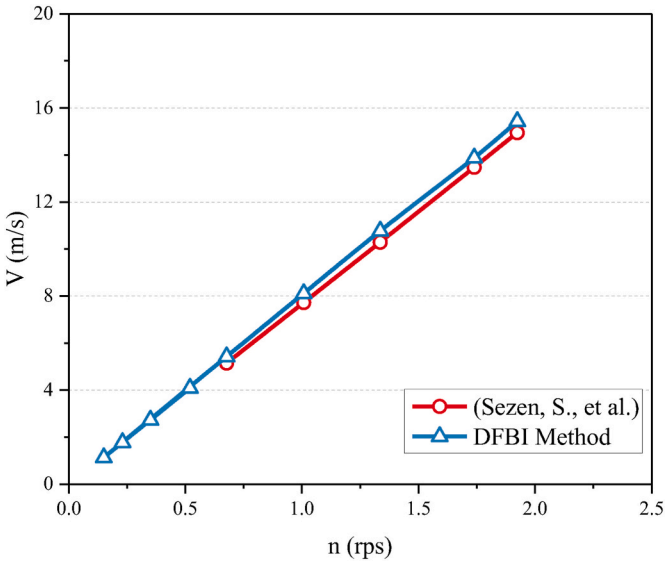

Fig. 11. The comparison of the full-scale DARPA Suboff AFF-8submarine self-propulsion points.

Comparing the numerical results obtained using the DFBI method with the other numerical simulation result, good agreement is observed, as shown in Fig. 11. The differences between the numerical and experimental results were approximately 5%, as shown in Table 5.

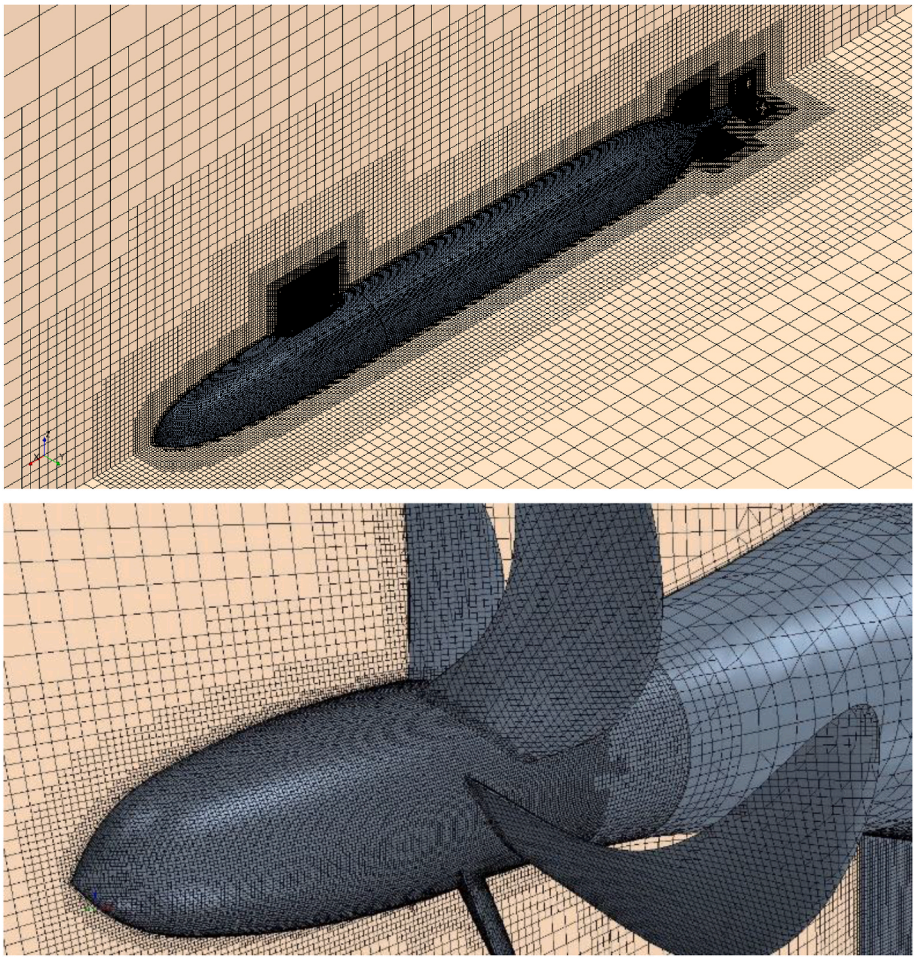

Fig. 10. Mesh view of the Full-scale DARPA Suboff AFF-8 submarine model with the INSEAN E1619 propeller model.

Table 5
The difference between the common method and DFBI method results for the full-scale DARPA Suboff AFF-8 submarine self-propulsion analysis.

Propeller Speed (rps)	Common Method – Advance Velocity (m/s) (Sezen et al.)	DFBI Method – Advance Velocity (m/s)	Difference
0.677	5.144	5.423	5.42%
1.008	7.717	8.107	5.06%
1.336	10.289	10.760	4.61%
1.739	13.473	13.878	3.02%
1.924	14.948	15.425	3.19%

Table 6
Grid independence studies.

Parameter	AUV
Fine Grid	4633230
Medium Grid	2528192
Coarse Grid	1662301
Resistance1	180.564
Resistance2	186.325
Resistance3	211.498
GCIfine	0.442 %

4. Hydrodynamics of the remora-inspired AUV

This section presents an investigation into the hydrodynamic performance of the remora-inspired AUVs. Based on a prior hydrodynamics study of the remora (Xu et al., 2021), the inspiration for the hull design was drawn from the posture of the remora fish docking on the shark. Two types of simulations were conducted in this section. The first type of simulation, the AUV free-stream analysis simulations, was performed as a benchmark to understand the individual hydrodynamic performances of the remora-inspired AUV. The second type was the AUV-flat plate attachment analysis simulations, which were conducted to investigate the hydrodynamic characteristics of the remora-inspired AUV under the developed boundary layer.

4.1. AUV in free-stream conditions

The hydrodynamic performance of the remora-inspired AUV in free-stream condition was evaluated through simulations, and the results can be considered as a benchmark for subsequent analyses. The same settings used in the resistance analysis in Section 3.1 were employed, including the computational domain, boundary conditions, and mesh generation, with confidence gained from the resistance simulation. Due to the significant size difference, a grid independence study was conducted to verify the simulation setup (Chen et al., 2008; Celik et al., 2008). Three different grid groups were used, including a coarse grid, a medium grid, and a fine grid, with a grid refinement ratio R of approximately 1.3. The grid parameters were kept fixed as percentages of the base size, while the grid size for the surface and volume mesh was varied by modifying the base size, except for the prism layer mesh. The numerical uncertainty values for the resistance were approximately 0.4425% for the AUV, as presented in Table 6. Based on the computational cost and accuracy, the medium grid was chosen for subsequent analyses. The cell count was 2.53 million and y+ was kept below 1, and the mesh view was shown in Fig. 12.

The velocities at the velocity inlet were set based on the results obtained from previous full-scale submarine self-propulsion simulations. The velocities selected for this study ranged from 1.126 to 8.107 m/s, and the simulation results from the free stream analysis were presented in Fig. 13.

4.2. AUV in fully developed boundary layer flow

Prior to the extensive numerical investigation of AUV docking to the

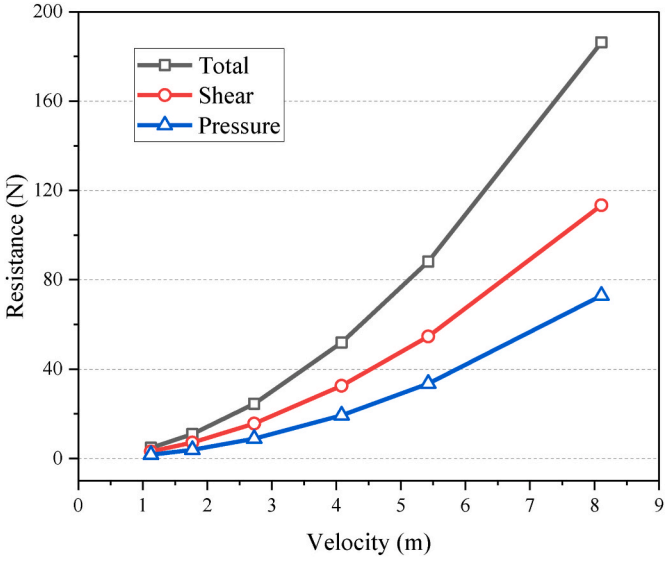

Fig. 13. The resistance of the remora-inspired AUV in the free stream.

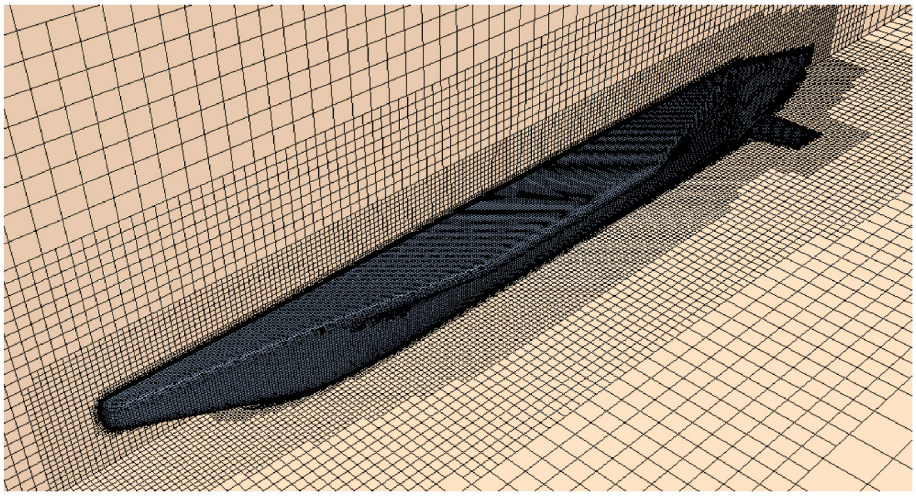

Fig. 12. Mesh view of the remora-inspired AUV model.

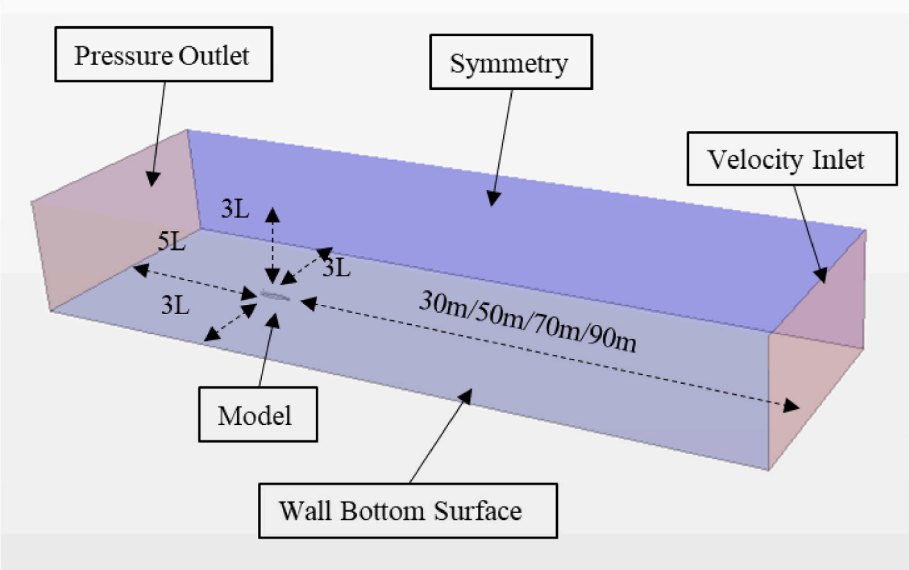

Fig. 14. Domain and boundary conditions of the AUV-flat plate attachment analysis.

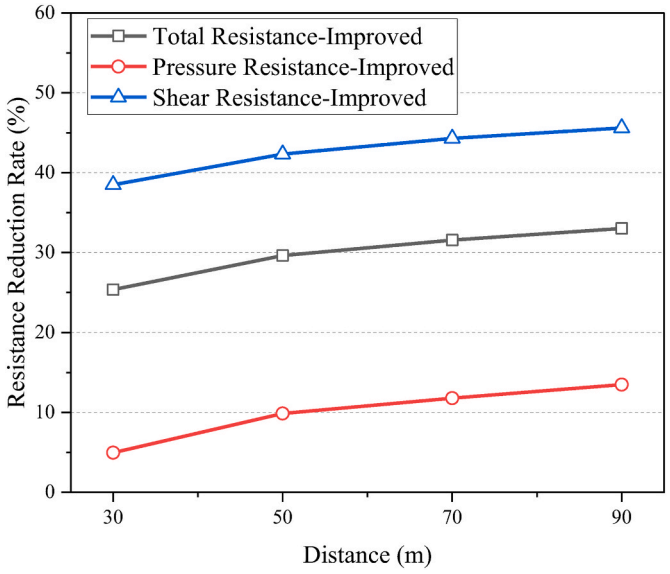

Fig. 15. The reduction rate of the resistance in flat plate attachment analysis compared to the AUV free-stream condition for the remora-inspired AUV at the different distances between the AUV model and the upstream inlet.

submarine, to investigate the hydrodynamic characteristics of the remora-inspired AUV, AUV docked onto a flat plate within a fully developed boundary layer flow has been investigated.

A relatively longer cuboid domain was created to develop the boundary layer flow, as Fig. 14 shows. The bottom surface was defined with a non-slip wall boundary condition to generate a range of developed boundary layer flows. The inlet was positioned 30 m/50 m/70 m/90 m upstream from the AUV model to produce various thicknesses of the boundary layer and was defined as a velocity inlet. The outlet was 5 L downstream from the model and was defined as a pressure outlet, while the top and sides surfaces were positioned 3 L from the model and were defined with symmetry boundary layer conditions. Regarding the mesh generation, the same setting was applied as previous simulations. The cell counts were 2.26–2.32 million, and the y+ was kept below 1 for the AUV model and the domain bottom.

A higher inflow velocity of 8.107 m/s was applied to the velocity inlet. This velocity value was determined based on the results of the full-scale submarine self-propulsion analysis simulation, which showed that the thickness of the boundary layer around the submarine could fully envelop the AUV model at a forward speed of 8.107 m/s.

The resistance of the AUV in the boundary layer flow is compared with the one in the free-stream condition. Figs. 15 and 16 demonstrate the results of the AUV-flat plate attachment analysis simulation for the remora-inspired AUV. The resistance reduction rates of the AUV is the percentage of resistance reduction comparing to the resistance in free stream. It increases with the increasing thickness of the boundary layer, with the total resistance reduction ranging from 25.36% to 33.03%, which is consistent with the expectation and aligns with the previous research (Xu et al., 2021). Additionally, Fig. 17 shows that there is no flow separation and vortices present in the stern of the AUV model. Consequently, this remora-inspired AUV model was used for the subsequent AUV-submarine attachment analysis.

5. Determination of the optimum docking locations & the Reynolds number affect

With the above remora-inspired AUV, the AUV-submarine attachment simulations were performed to investigate the hydrodynamic characteristics of the AUV attached to various locations of the submarine. Then, the Reynolds number affect has been investigated with the AUV docked to the identified optimal docking locations.

5.1. Identification of the optimum docking locations

According to the previous research (Xu et al., 2021), remora-inspired AUV would favour fully developed boundary layer flow and adverse pressure gradient to achieve maximum resistance reduction to save energy. So to identify the best docking location for the developed AUV, this simulation has been conducted.

During this simulations, the inflow velocity was set to 8.107 m/s, which is the design speed of the submarine and is consistent with the previous study. Velocity contours of low-velocity regions were extracted from the full-scale self-propulsion simulation, as shown in Fig. 18. The boundary layer gradually develops along the hull. The thickness of the boundary layer increases first, but near the stern region the boundary layer thickness reduces due to the suction generated by the propeller. In addition, a large area of low velocity is developed behind the submarine sail.

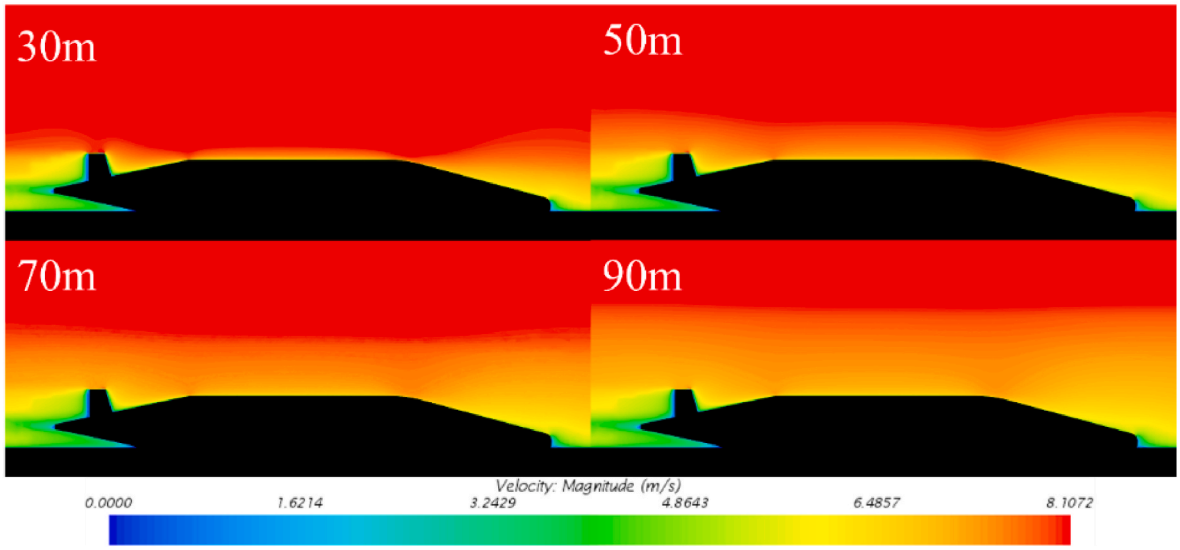

Fig. 16. The velocity contours of the AUV-flat plate analysis for the remora-inspired AUV.

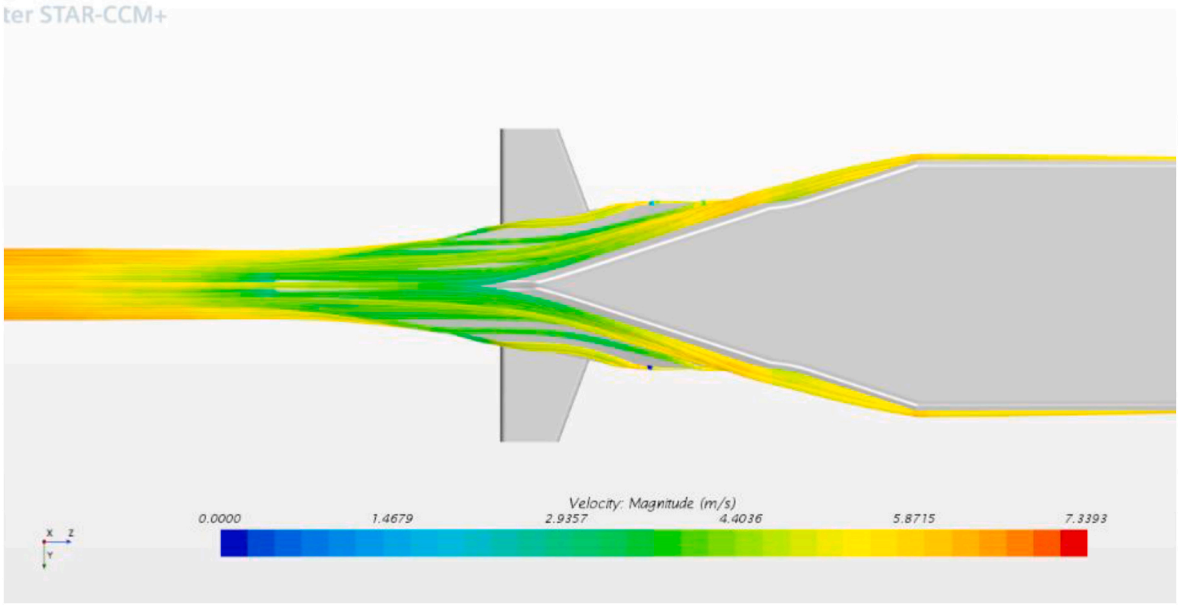

Fig. 17. The streamline behind the stern of the remora-inspired AUV.

Nine potential docking locations on the submarine surface were identified using the self-propulsion simulation in Section 3.3. In the longitudinal direction, three cross-sections (designated as A, B, and C in Fig. 18) were chosen at the distances of 65 m, 45 m, and 27 m upstream of the stern of the submarine, respectively. In each cross section, three positions were selected which were on the top, side, and bottom of the submarine. Table 7 presents the thickness of the low-velocity regions and the ratio between its thickness and the height of the AUV for various attachment locations. The B section exhibited a thicker boundary layer than other positions.

Figs. 19 and 20 presents the results of the total resistances and resistance reduction rates when the developed AUV docks to the above identified locations. The B-side achieves the highest total resistance reduction rate of 35.23%. Furthermore, all attachment locations in the B section exhibits a slightly lower total resistance compared to other sections. Combining to the comparison of boundary layer thickness shown in Tables 7 and it is consistent with the previous finding in Section 4.2 that the resistance reduction is caused by the thicker boundary layers.

Regarding the top locations of section A and B, despite their location within a large low-velocity region generated by the sail of the submarine, they do not show any significant advantage. For the C section, it doesn't show any significant resistance reduction.

Furthermore, to understand the rationale of the resistance reduction, as shown in Figs. 21 and 22, shear and pressure components of resistance have been extracted and compared. The attachment location has less impact on the shear resistance but significant effect on the pressure resistance. The pressure resistance in the C section increased significantly due to its proximity to the stern of the submarine, where a non-negligible suction force was generated by the motion of the propeller behind the stern. Concerning the A and B sections, the reduction effects in the pressure resistance are similar, while the side and bottom locations have higher reduction than the top location.

In order to understand the resistance reduction mechanism, further

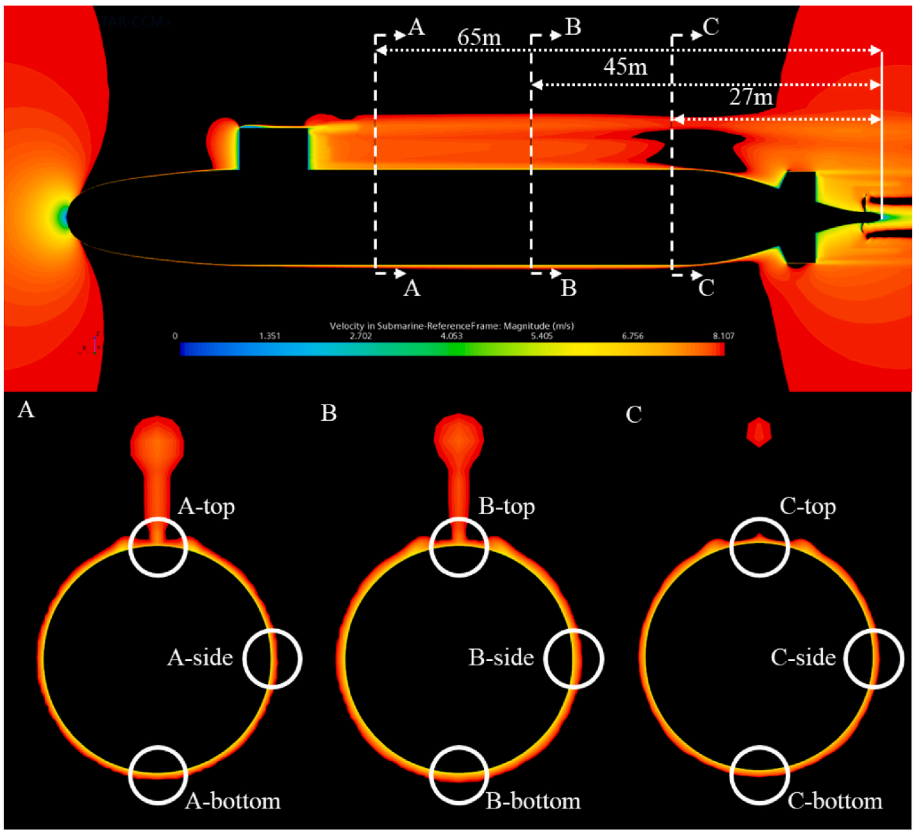

Fig. 18. The low-velocity regions in the vicinity of a full-scale DARPA Suboff AFF-8 submarine model in self-propulsion condition.

Table 7
The thickness of the low-velocity regions in different attachment locations in the self-propulsion of the submarine.

	A	B	C
Top	6.984 (3325.76%)	7.116 (3388.76%)	0.539 (256.85%)
Side	0.362 (172.38%)	0.526 (250.67%)	0.392 (186.57%)
Bottom	0.370 (176.22%)	0.525 (250.03%)	0.385 (183.20%)

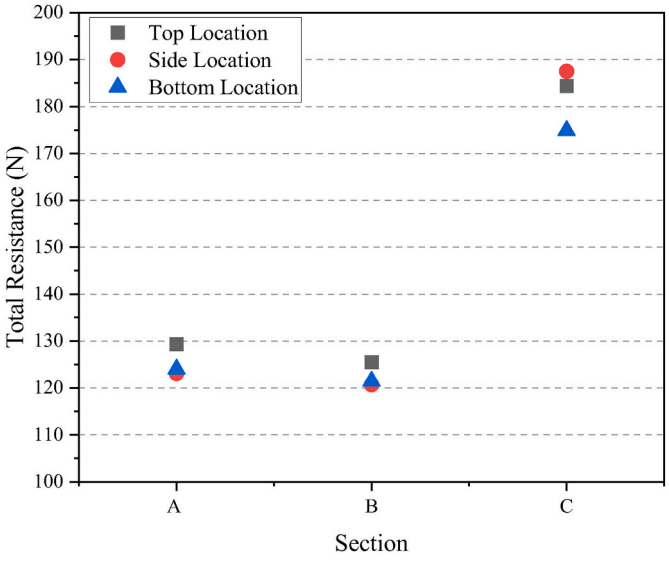

Fig. 19. The comparison of the total resistances for different attachment locations.

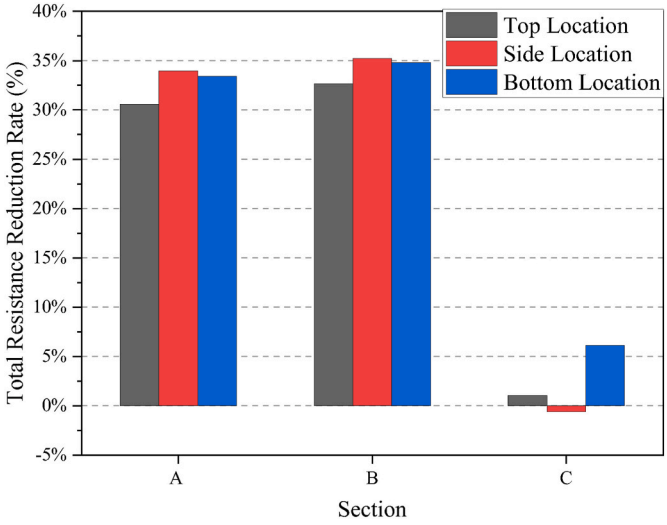

Fig. 20. The comparison of the total resistance reduction rate for different attachment locations.

detailed flow analysis has been conducted. Fig. 23, Figs. 24 and 25 show the velocity contours around the remora-inspired AUV at different docking locations in sections A, B and C. As shown in Fig. 23, at the top position, a thinner boundary layer is observed on two sides of the AUV (area 1) due to the affect of main sail. And two high-pressure regions are present on the top of the AUV hull (area 2 in Fig. 23), with this phenomenon being more pronounced in the proximity of the sail (A section). The thickness of the boundary layer is the greatest in the B section shown in Fig. 24, which is in agreement with the results of the submarine self-propulsion analysis. Additionally, the velocity distributions

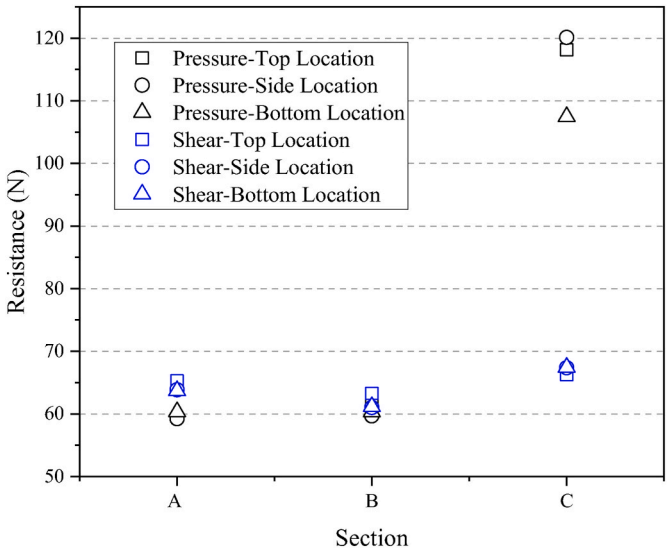

Fig. 21. The comparison of the pressure and shear resistances for different attachment locations.

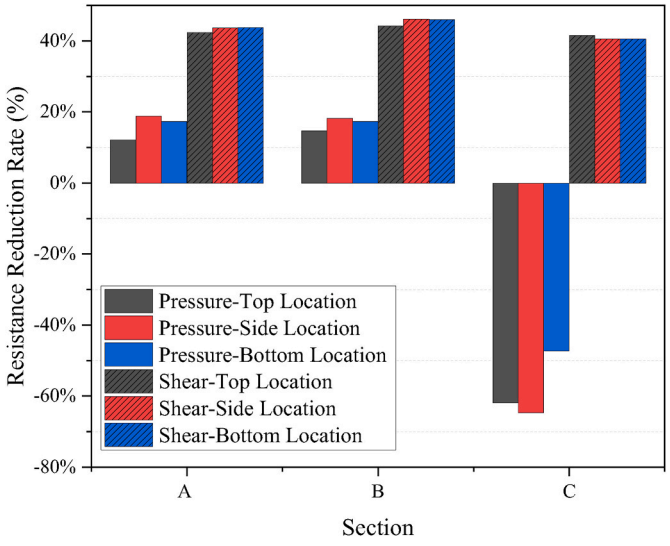

Fig. 22. The comparison of the pressure and shear resistance reduction rates for different attachment locations.

around the AUV at the side location were similar to those at the bottom locations in all sections. Furthermore, the velocity contours in the C section (Fig. 25) demonstrate that the boundary layer is influenced as expected by the propeller, gradually thinning at all attachment locations in the C section.

According to the above investigations, it is evident that all attachment locations in the C section are unsuitable for the AUV docking operation. This is due to the suction force generated by the motion of the propeller, which significantly increases the pressure resistance on the AUV, resulting in almost no reduction in resistance. In addition, due to the complex structure of the submarine's stern and the proximity of this docking area to the propeller, the risk of the AUV docking operation will increase.

In terms of the attachment location in the A section, a lower total resistance reduction is observed compared to the B section. It is noteworthy that although the A-top and B-top attachment locations are both located in the low-velocity region, they provide a lower total resistance reduction than the side and bottom attachment locations. There seems to be no effective adverse pressure gradient region generated behind the sail of the submarine for a remora-inspired AUV of this size. In addition, the wake behind the sail will increase the difficulty of controlling the AUV.

For the attachment locations in the B section of the submarine's middle hull, the highest total resistance reduction can be achieved at the B-side attachment location, with a reduction rate of up to 35.23%. However, the B-bottom attachment location also provides a resistance reduction effect close to that of the B-side attachment location, at 34.81%. Additionally, the B-side attachment location requires the AUV to be rotated 90° for the docking operation, which increases the energy consumption and control difficulty of the AUV. Therefore, the B-bottom attachment location is considered more advantageous than other attachment locations. However, it should be noted that certain submarines can rest on the seabed conducting surveillance missions. In such operations, it is not allowed for the AUV to attach onto the submarine bottom. This specific condition must be carefully considered during the design and operation of the dynamic underwater recovery mechanism for the AUV.

5.2. *The effect of the forward velocity and hence the Reynolds number*

Based on the above analysis of the attachment locations, the B-bottom attachment location is selected to investigate the effect of the advance velocity of the submarine. Five velocities were simulated in this study, namely 5.423 m/s, 4.081 m/s, 2.727 m/s, 1.769 m/s, and 1.126 m/s.

It can be seen from Fig. 26 that the thicknesses of the boundary layers are nearly identical across this range of velocities. In addition, Fig. 27 shows the resistance reduction rates for the AUV attached to the submarine at different velocities. As the velocity reduces, the resistance reduction of the AUV attached to the submarine increases slightly from 34.79% to 38.52%. Therefore, in terms of the resistance reduction, the effect of Reynolds number is not significant.

6. AUV-submarine interaction analysis: approaching & docking

Based on the above study, the optimal docking location can be identified for the selected submarine hull. To further investigate the challenge when docking an AUV to the submarine, further analysis has been conducted to research the process of the docking and the forces experienced in the docking process, shown in Fig. 28.

The study simulates AUV moves from 2 L (length of the AUV) away from the submarine to the attachment location. The B-bottom attachment location, as determined in the previous section, was chosen as the docking position. Considering the speed range of the general AUVs, a velocity of 2.727 m/s was selected as the docking velocity. The same horizontal velocity has applied to both the submarine and the AUV and then a constant vertical force presenting the additional thrust needed to dock the AUV was applied to the AUV model to drive the AUV towards the submarine. The Dynamic Fluid Body Interaction (DFBI) module was employed and only the translational motion is enabled to allow the AUV approaching and docking to the submarine while maintaining the course with the submarine illustrated in Fig. 29. The submarine and the AUV were assumed as rigid body with no deformation when contacting. To avoid zero or negative volume cells the motion was limited to the closest 3 mm to the submarine surface and a dumping length of 1 cm was applied to model the contact.

In this study, five different and constant vertical forces were applied: 25 N, 50 N, 75 N, 100 N and 125 N. Through the numerical simulations, the study aimed to understand the variation in the hydrodynamic characteristics of the AUV as it approaches the bottom of the submarine, and the effect of the different velocities during the docking process.

In this numerical simulation, the vertical motion of the AUV model was enabled after 60 s, ensuring that the boundary layer of the submarine was fully developed. A video has been attached in the paper to

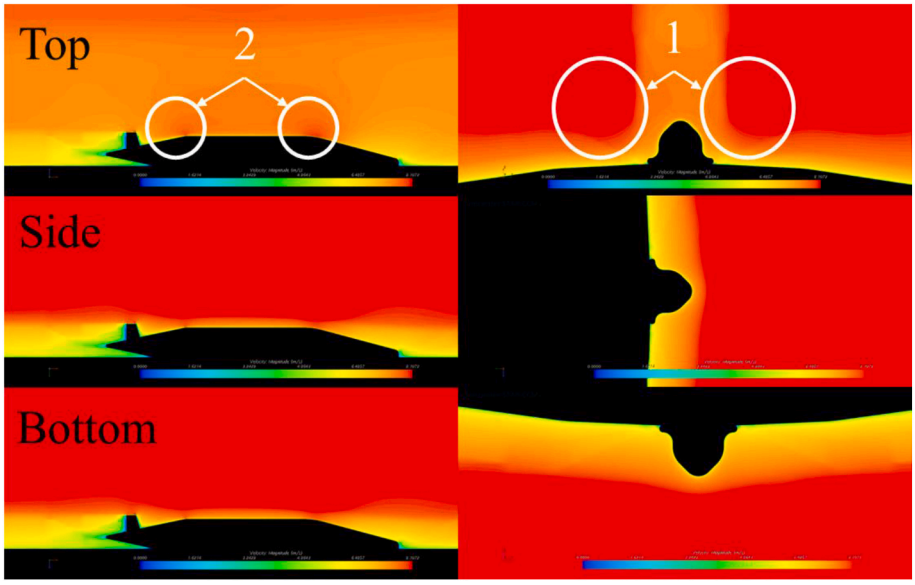

Fig. 23. The velocity contours at three attachment locations of the A section in AUV-submarine attachment analysis simulations.

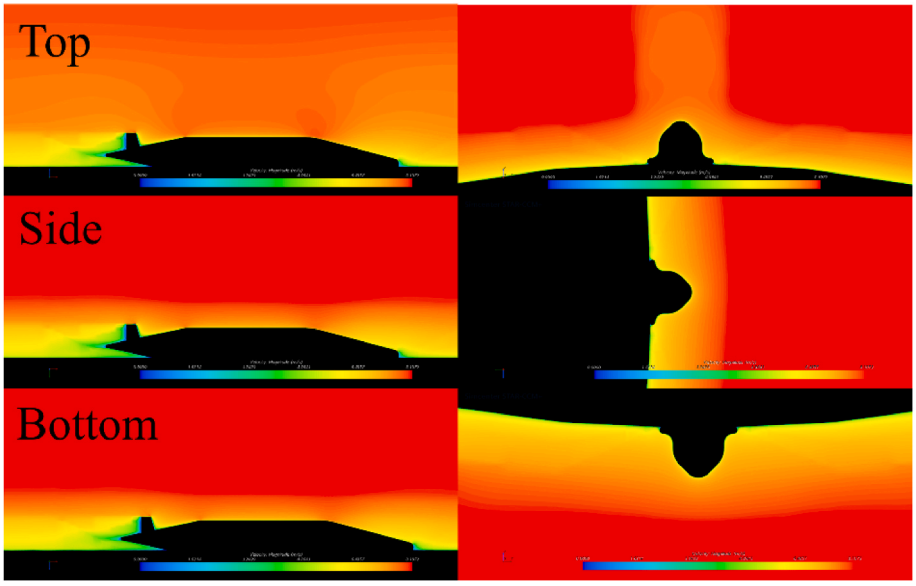

Fig. 24. The velocity contours at three attachment locations of the B section in AUV-submarine attachment analysis simulations.

show the approaching and docking process (Video Attachment 1). And Fig. 30 shows the velocity contours during the docking process, where the flow characteristics around the AUV can be observed. When the AUV reaches the boundary layer of the submarine, the boundary layer flow of the submarine and the flow around the AUV interact. It is very interesting to notice that due to this interaction the boundary layer thickness is reduced after the AUV docks to the submarine.

In Fig. 31, the resistance of the AUV is monitored through this docking process. As the AUV entered the boundary layer of the submarine, the resistance began to decrease (A in Fig. 31). This gradual decrease is disrupted, when the AUV approaches very close to the docking position. A significant fluctuation is occurred (B in Fig. 31) with a sudden increase in resistance and a sudden decrease follows. Thereafter, the resistance continues to reduce, and finally, it reduces by 29.09% compared to the resistance in the free stream condition.

To understand this process in detail, the force, velocity, acceleration and position were monitored in the vertical direction. Fig. 32 shows the case driving by the constant 50 N vertical force. The vertical force resulting from the fluid force, as well as the AUV vertical acceleration, velocity and displacement are illustrated. Six stages involved in the docking process can be seen as follows.

A. **Start**: The AUV started to accelerate due to the constant vertical force applied until the equilibrium state was achieved.
B. **Approach**: The AUV maintained a constant speed towards the submarine until it approached the boundary layer of the submarine.
C. **Enter**: The AUV began to enter the boundary layer of the submarine. The vertical velocity drops.
D. **Contact**: It took approximately 0.5 s for the AUV to reach the designated docking position after entering the boundary layer. A sudden acceleration and a contact with the submarine can be observed with velocity zeroing. An impact force can be seen, peaking at 1160.4 N.

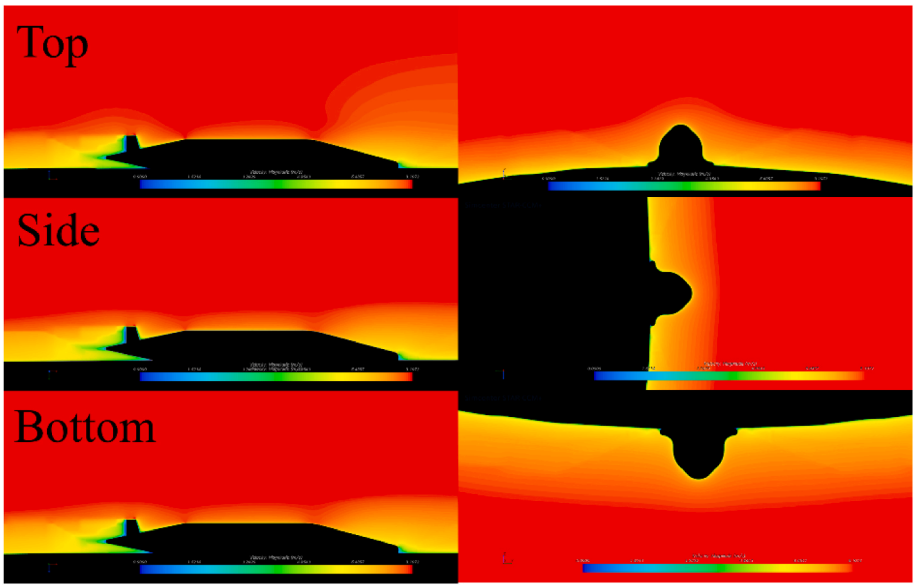

Fig. 25. The velocity contours at three attachment locations of the C section in AUV-submarine attachment analysis simulations.

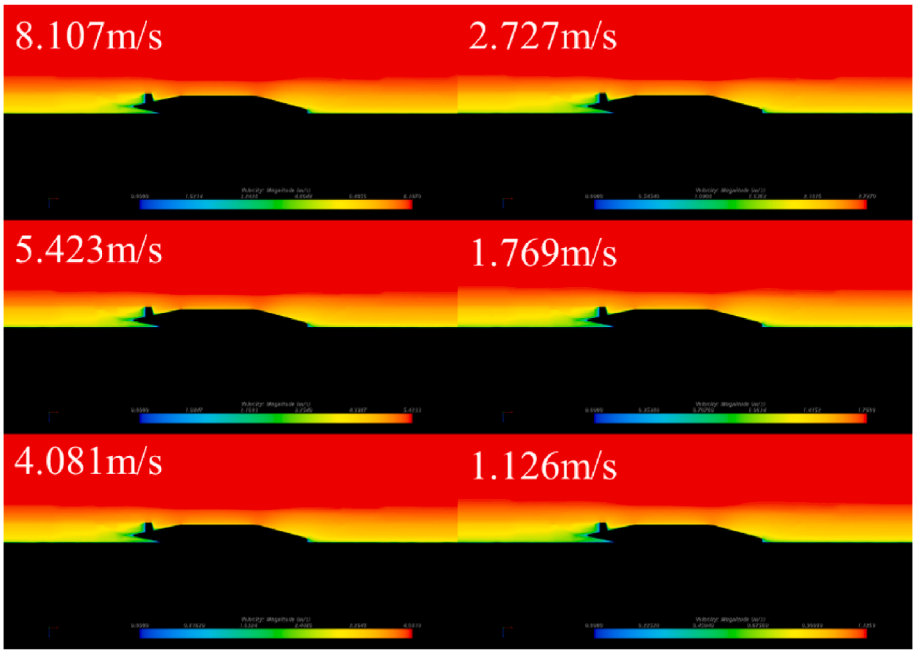

Fig. 26. The velocity contours of AUV-submarine attachment analysis simulations when the AUV attached to the B-bottom location at various velocities.

E. **Bounce**: After the contact, as shown in the displacement plot, the AUV bounces on the submarine surface but immediately is sucked back to the surface due to the large suction force generated between the AUV and the submarine.
F. **Attach:** The small bouncing phenomenon is soon ceased and the AUV is sucked to the submarine. No more additional vertical force is needed to keep the AUV close to the submarine. A constant suction force can be observed generated by the flow, approximately at 19 N.

The above simulation shows it is feasible to drive the AUV to the submarine and attach onto the submarine surface. For the impact force, the contact area between the submarine and the AUV is 0.3 m^2, and the maximum pressure is 3868 Pa. The submarine and the AUV are not experiencing an impact force which would cause potential damages (Do et al., 2022; Lin et al., 2022; Pan and Zhang, 2021). And after the docking, no additional vertical force is required to prevent the AUV from moving away from the submarine, as the suction force can be generated by the fluid flow.

In order to understand the minimum vertical force required, the minimum impact force and also effect of different vertical driving force, simulations were conducted under different constant vertical forces of 25 N, 75 N, 100 N, and 125 N, and the results were presented in Fig. 33. It can be seen that the phenomena are very similar with each other under the various forces applied. The only difference observes in the study is that, during stages C and D under a constant vertical force of 25 N, as marked by a blue circle in Fig. 33 a velocity fluctuation has occurred when the AUV entered the boundary layer of the submarine. But the AUV still manages to dock to the submarine.

As the applied force increased, the time required for docking decreased, and the impact force increased, as shown in Fig. 34. For all

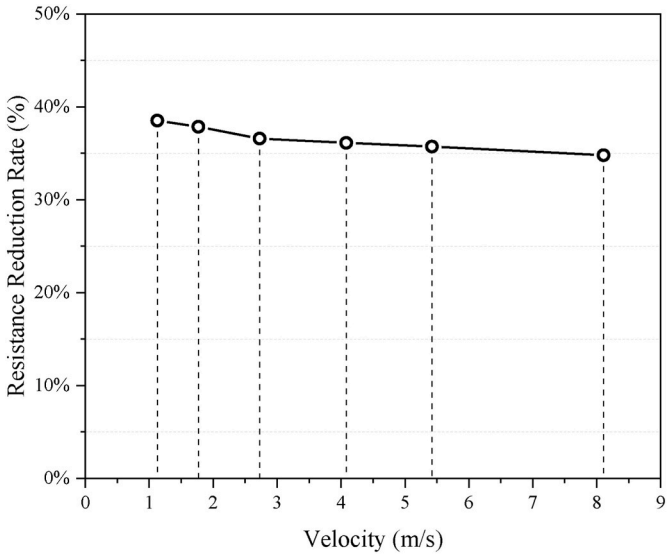

Fig. 27. The total resistance reduction rates when the remora-inspired AUV attached to the B-bottom attachment location at different velocities.

cases, after the AUV reached the docking position, the fluid forces sucking it onto the submarine are all approximately 19 N across all the cases.

7. Conclusions

This paper presents an investigation into the hydrodynamic characteristics of a remora-inspired AUV docking to a full-scale self-propelled submarine. The paper first researches into the design of the remora-inspired AUV and then investigated the potential location and strategy of the AUV docking to the submarine. Afterwards, the paper presented a full-coupled analysis of the AUV docking to the designated location. Following key findings are listed below.

1. The remora-inspired AUV hull form is first time developed and evaluated using computational fluid dynamics.
2. Through the investigation of the hydrodynamics characteristics of the remora-inspired AUV, the AUV-flat plate attachment analysis reveals a significant reduction in resistance, ranging from 25.36% to 33.03% as the thickness of the boundary layer increases, which is in line with the previous research and the expectations.
3. To identify the optimum docking location to the submarine, a full-scale self-propulsion submarine is simulated using CFD. 3 potential longitudinal positions with 3 potential circumferential locations have been evaluated.
4. AUV docking onto the above 9 potential locations has evaluated. Combining the resistance reduction effect and the practical operational feasibility, the location at the bottom of the middle section is recommended. And the resistance reduction of the AUV remains almost constant for velocities ranging between 1.126 m/s and 8.107 m/s, ranging from 38.52% to 34.79%.
5. Fully coupled analysis has been conducted to research the hydrodynamics in the docking process. The resistance of the AUV decreases as it enters the boundary layer of the submarine, which is expected.
6. The docking processes with constant vertical forces applied on the AUV consist six stages: start, approach, enter, contact, bounce and attach. Docking time and impact force have been analysed and shorter docking time will result in higher impact force.
7. After the docking process, the AUV doesn't require additional vertical thrust force as the fluid force sucks the AUV towards the submarine.

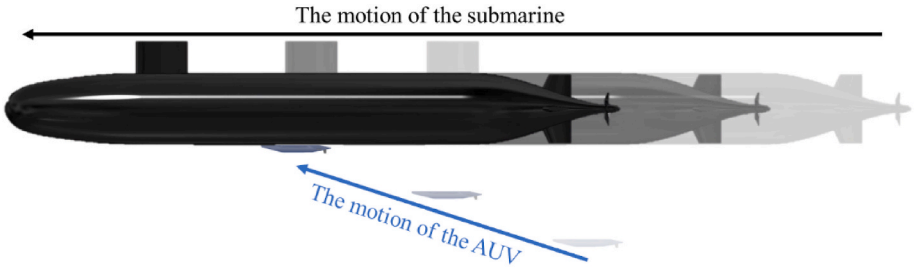

Fig. 28. The motion of the AUV and the submarine during docking operation.

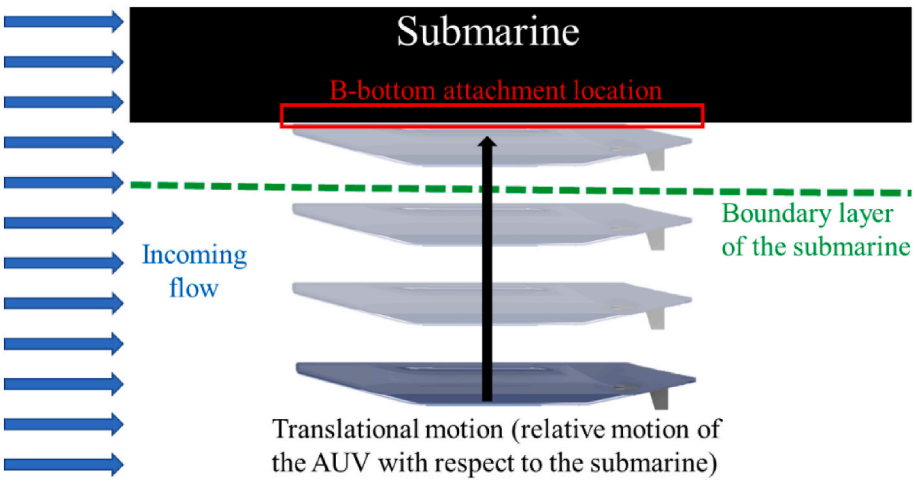

Fig. 29. The relative motion of the AUV model with respect to the submarine model.

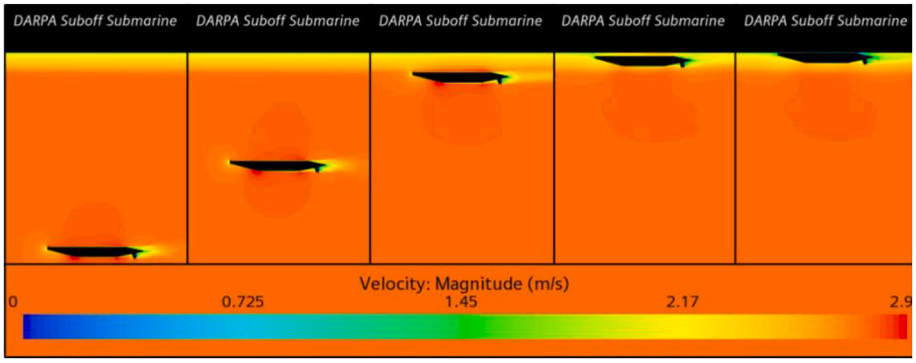

Fig. 30. The velocity contours during the motion of the AUV.

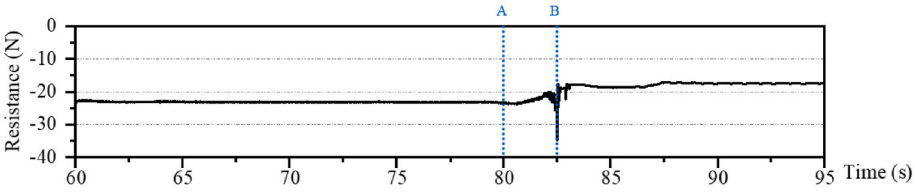

Fig. 31. The resistance of the AUV in the docking process with a 50 N constant vertical force applied.

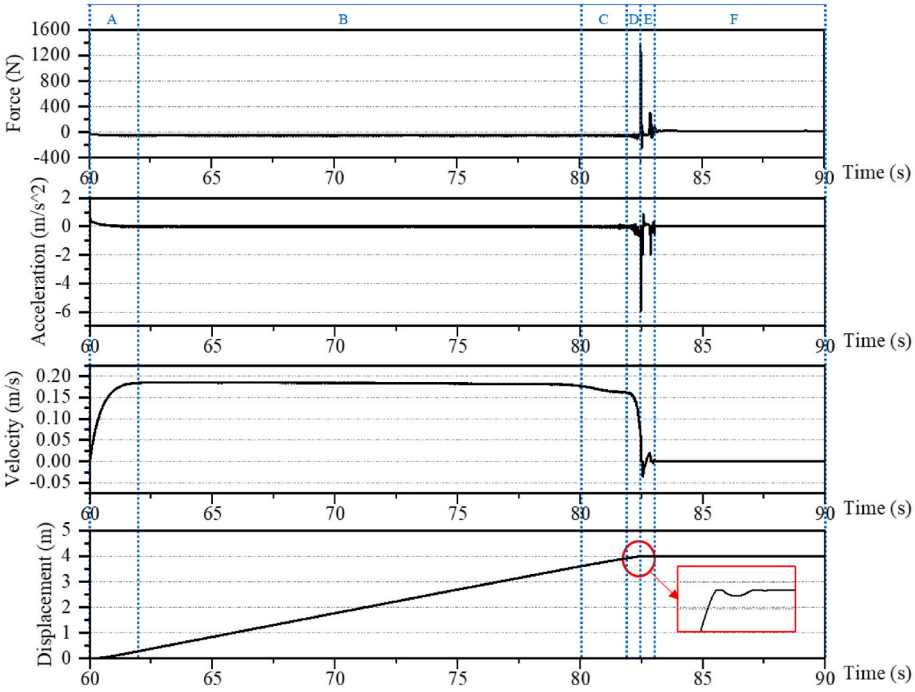

Fig. 32. The different stages of the docking process of the remora-inspired AUV with the 50 N vertical constant force.

Based on the investigation of the remora-inspired AUV docking onto the submarine, it shows the forces needed to dock the AUV onto the submarine. And it is numerically evidenced to be feasible to perform such operation. Following this research, further confidence has been gained to develop prototype of such bio-inspired AUV.

CRediT authorship contribution statement

Yunxin Xu: Conceptualization, Numerical simulation, Investigation, Validation, Visualization, Writing – original draft, Writing – review & editing. **Weichao Shi:** Conceptualization, Methodology, Writing – original draft, Writing – review & editing, Resources, Supervision, Project administration, Funding acquisition. **Yang Song:** Formal analysis, Investigation, Writing – review & editing. **Hongbo Hou:** Numerical simulation, Validation, Investigation, Writing – review & editing.

Declaration of competing interest

The authors declare that they have no known competing financial interests or personal relationships that could have appeared to influence the work reported in this paper.

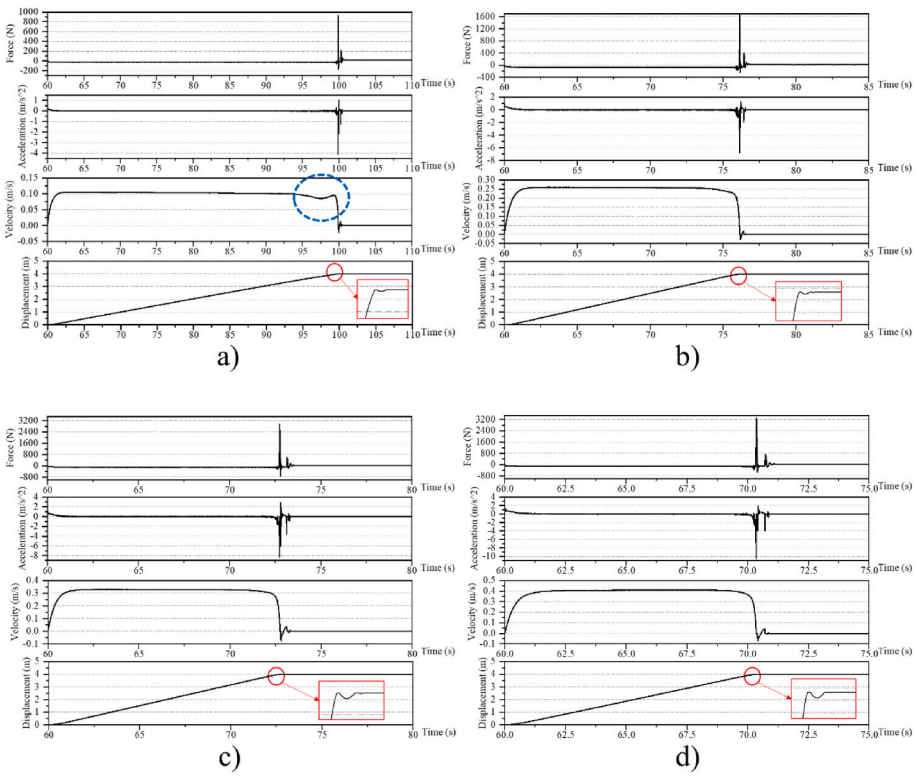

Fig. 33. The different stages of the docking process of the remora-inspired AUV with the vertical constant forces, a) the case of 25 N vertical constant force applied, b) the case of 75 N vertical constant force applied, c) the case of 100 N vertical constant force applied and d) the case of 125 N vertical constant force applied.

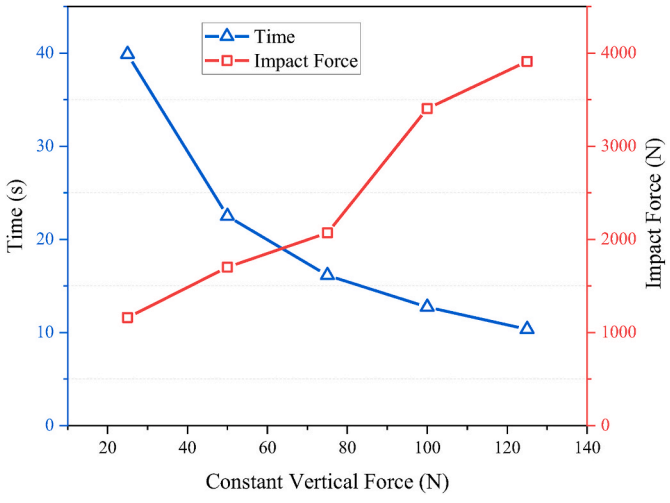

Fig. 34. The impact forces when the AUV reached the docking position and the time required under different vertical constant forces.

Data availability

Data will be made available on request.

Acknowledgements

Results were obtained using the ARCHIE-WeSt High Performance Computer (www.archie-west.ac.uk) based at the University of Strathclyde.

Appendix A. Supplementary data

Supplementary data to this article can be found online at https://doi.org/10.1016/j.oceaneng.2023.116447.

References

Beckert, M., Flammang, B.E., Anderson, E.J., Nadler, J.H., 2016. Theoretical and computational fluid dynamics of an attached remora (Echeneis naucrates). Zoology 119 (5), 430–438.

Brunnschweiler, J.M., 2006. Sharksucker-shark interaction in two carcharhinid species. Mar. Ecol. 27 (1), 89–94. https://doi.org/10.1111/j.1439-0485.2005.00052.x.

Celik, I.B., Ghia, U., Roache, P.J., Freitas, C.J., 2008. Procedure for estimation and reporting of uncertainty due to discretization in CFD applications. Journal of fluids Engineering-Transactions of the ASME 130 (7).

Chase, N., Carrica, P.M., 2013. Submarine propeller computations and application to self-propulsion of DARPA Suboff. Ocean Eng. 60, 68–80.

Chen, K., Huang, D.-b., Li, Y.-b., 2008. Grid convergence study in the resistance calculation of a trimaran. J. Mar. Sci. Appl. 7 (3), 174–178. https://doi.org/10.1007/s11804-008-7065-1.

Di Felice, F., Felli, M., Liefvendahl, M., Svennberg, U., 2009. Numerical and experimental analysis of the wake behavior of a generic submarine propeller. Prism 1 (8), 158.

Do, Q.T., Muttaqie, T., Nhut, P.-T., Vu, M.T., Khoa, N.D., Prabowo, A.R., 2022. Residual ultimate strength assessment of submarine pressure hull under dynamic ship collision. Ocean Eng. 266, 112951.

Fernandes, V.H., Neto, A.A., Rodrigues, D.D., 2015. Pipeline inspection with AUV. In: 2015 IEEE/OES Acoustics in Underwater Geosciences Symposium (RIO Acoustics). IEEE, pp. 1–5.

Forrest, A.L., Laval, B.E., Pieters, R., Lim, D.S., 2008. Convectively driven transport in temperate lakes. Limnol. Oceanogr. 53 (5part2), 2321–2332.

Hardy, T., Barlow, G., 2008. Unmanned Underwater Vehicle (UUV) Deployment and Retrieval Considerations for Submarines.

Hayashi, E., et al., 2013. Customizing an Autonomous Underwater Vehicle and developing a launch and recovery system. In: 2013 IEEE International Underwater Technology Symposium (UT). IEEE, pp. 1–7.

Heo, J., Kim, J., Kwon, Y., 2017. Technology development of unmanned underwater vehicles (UUVs). J. Comput. Commun. 5 (7), 28.

ITTC, 2011. Practical guidelines for ship CFD applications. In: *26th* ITTC, Hague, p. 18.

Kemna, S., Hamilton, M.J., Hughes, D.T., LePage, K.D., 2011. Adaptive autonomous underwater vehicles for littoral surveillance: the GLINT10 field trial results. Int. serv. robot. 4, 245–258.

Leong, Z.Q., Ranmuthugala, D., Penesis, I., Nguyen, H., 2015. Quasi-static analysis of the hydrodynamic interaction effects on an autonomous underwater vehicle operating in proximity to a moving submarine. Ocean Eng. 106, 175–188.
Lin, M., et al., 2022. Docking to an underwater suspended charging station: systematic design and experimental tests. Ocean Eng. 249, 110766.
Liu, H.-L., Huang, T.T., 1998. Summary of DARPA SUBOFF Experimental Program Data. NAVAL SURFACE WARFARE CENTER CARDEROCK DIV BETHESDA MD HYDROMECHANICS.
Menter, F.R., 1994. Two-equation eddy-viscosity turbulence models for engineering applications. AIAA J. 32 (8), 1598–1605.
Nicholson, J., Healey, A., 2008. The present state of autonomous underwater vehicle (AUV) applications and technologies. Mar. Technol. Soc. J. 42 (1), 44–51.
Pan, W., Zhang, Y., 2021. Research on dynamic docking process and collision problems of AUV based on joint control simulation. In: 2021 7th International Conference on Computer and Communications (ICCC). IEEE, pp. 1057–1061.
Roddy, R.F., 1990. Investigation of the Stability and Control Characteristics of Several Configurations of the DARPA SUBOFF Model (DTRC Model 5470) from Captive-Model Experiments. David Taylor Research Center Bethesda MD Ship Hydromechanics Dept.
Sarda, E.I., Dhanak, M.R., 2016. A USV-Based automated launch and recovery system for AUVs. IEEE J. Ocean. Eng. 42 (1), 37–55.
Schofield, O., et al., 2007. Slocum gliders: robust and ready. J. Field Robot. 24 (6), 473–485.
Sezen, S., Dogrul, A., Delen, C., Bal, S., 2018. Investigation of self-propulsion of DARPA Suboff by RANS method. Ocean Eng. 150, 258–271.
Sezen, S., Delen, C., Dogrul, A., Atlar, M., 2021. An investigation of scale effects on the self-propulsion characteristics of a submarine. Appl. Ocean Res. 113, 102728.
Silva Jr., J.M., Sazima, I., 2006. Whalesuckers on spinner dolphins: an underwater view. JMBA2–Biodivers. Records.
Singh, H., et al., 2001. Docking for an autonomous ocean sampling network. IEEE J. Ocean. Eng. 26 (4), 498–514.
Singh, H., Fletcher, D.F., Nijdam, J.J., 2011. An assessment of different turbulence models for predicting flow in a baffled tank stirred with a Rushton turbine. Chem. Eng. Sci. 66 (23), 5976–5988.
ITTC, 2008. Testing and Extrapolation Methods. Procedure 7.5-02-03-01.1, Revision 02.
STAR-CCM+guidelines, "STAR-CCM+ Documentation.".
Venkatesan, S., 2016. AUV for Search & Rescue at sea-an innovative approach. In: 2016 IEEE/OES Autonomous Underwater Vehicles (AUV). IEEE, pp. 1–9.
Xu, Y., Shi, W., Arredondo-Galeana, A., Mei, L., Demirel, Y.K., 2021. Understanding of remora's "hitchhiking" behaviour from a hydrodynamic point of view. Sci. Rep. 11 (1), 1–20.
Zhang, H., et al., 2013. The general design of a seafloor surveying AUV system. In: 2013 OCEANS-San Diego. IEEE, pp. 1–5.